Analysis of Lamb Waves in Sea Ice

A thesis submitted in partial fulfillment of the requirements for the degree of Bachelor of Science degree in Physics from the College of William and Mary

by

Daniel Duane

Advisor: Mark Hinders

Senior Research Coordinator: Gina Hoatson

Date: April 24, 2015

Abstract

Cleanup crews have difficulty recovering oil slicks trapped under ice, because oil-detecting underwater drones cannot relay their position from under the ice. We are developing a system where an underwater drone releases a bouyant acoustic emitter when it finds oil, allowing cleanup crews to triangulate the location of the oil. We modeled the behavior of Lamb waves through ice plates, which will allow us to develop a system for automatically triangulating the source of the acoustic emitter. By varying the range of possible longitudinal and shear velocities of arctic ice, we were able to generate dispersion curves for group velocity and phase velocity as a function of plate frequency-thickness product. We focused our analysis on the zeroth order symmetric mode, which flattens as frequency-thickness product approaches zero, allowing for a system where slight changes in plate thickness will not alter the phase velocity and group velocity. We also used Finite Difference Time Domain software to model the behavior of the sound waves in the water, ice, and air.

1 Introduction

In 2010, an explosion in the Deepwater Horizon oil rig released an estimated 4.9 million barrels of oil in the Gulf of Mexico [1]. It is important to develop a system for locating oil slicks after a such spills, so the oil can be removed in order to minimize damage to the environment. Autonomous Underwater Vehicles (AUVs) can identify oil slicks using acoustic backscattering [2]. However, an AUV cannot remotely communicate its position in polar regions where ice covers the water, because GPS does not work under ice.

We are building a system for locating oil spills under an ice floe using an AUV. When the AUV detects an oil spill, it releases an underwater acoustic identification (UWID) tag, a buoyant, volleyball-sized device that emits acoustic waves (Figure 1). Once released, the UWID tag floats to bottom of the ice floe and generates a Lamb wave that spreads radially in the ice. In this scenario, the cleanup crew would know the general vicinity of the oil spill, and the members of the crew would scatter a series of GPS-enabled LD-GRIDSAT transponders on the surface of the ice (Figure 2). The LD-GRIDSATs would be able to detect the acoustic pulse in the ice as it propagates radially, allowing the system to automatically triangulate the origin of the UWID tag and the oil slick. Conceptual diagrams of the UWID tag and the LD-GRIDSAT tags are shown in Figure 3. This system will allow cleanup crews to isolate oil spills under ice.

An in-depth analysis of Lamb waves will be necessary to develop a system that use the properties of sea ice to accurately triangulate the location of an acoustic source under ice. This research project has two parts. In the first part, we used a MATLAB software package to create Lamb wave dispersion curves for sea ice in order to predict the proper angle of incidence for the acoustic emitter under the ice. In the second part, we used Finite Difference Time Domain (FDTD) elastic wave equation code to model the behavior of acoustic waves in the ice and in the surrounding water.

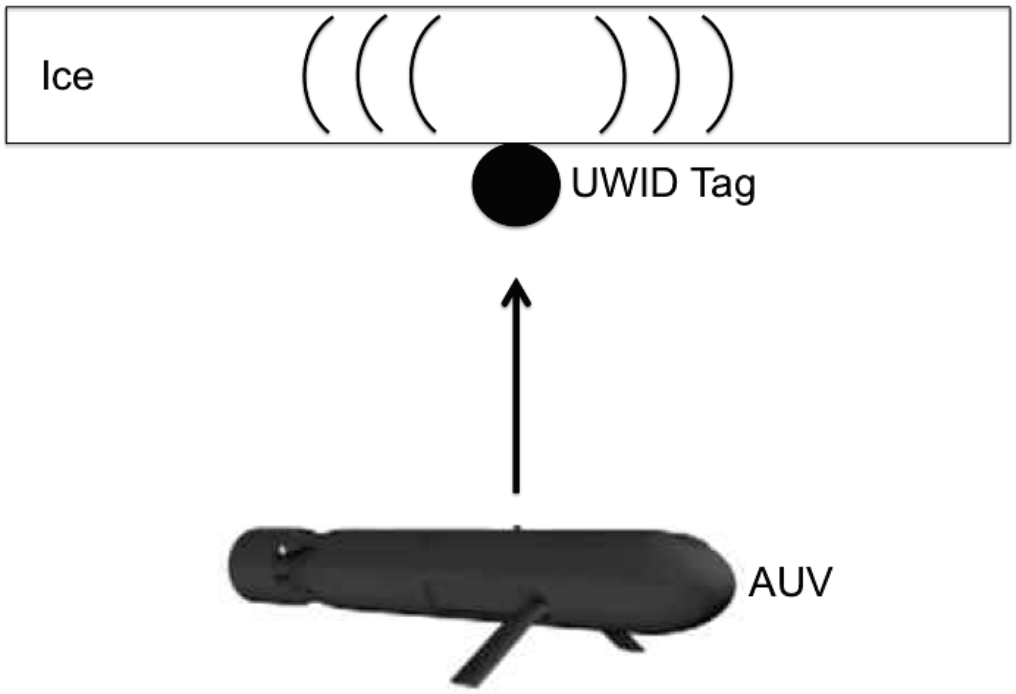

Figure 1: The AUV releases the UWID tag, which floats to the bottom of the ice and emits an acoustic wave.

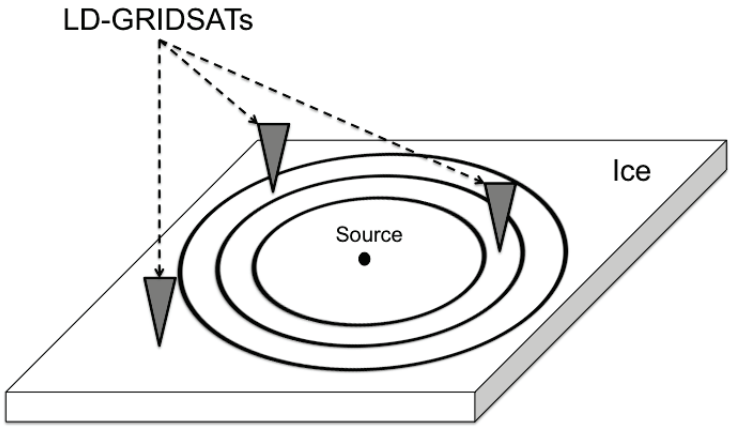

Figure 2: The GPS-enabled LD-GRIDSAT tags detect the acoustic pulse, allowing the cleanup crew triangulate the source of the acoustic pulse, and with it, the underwater oil.

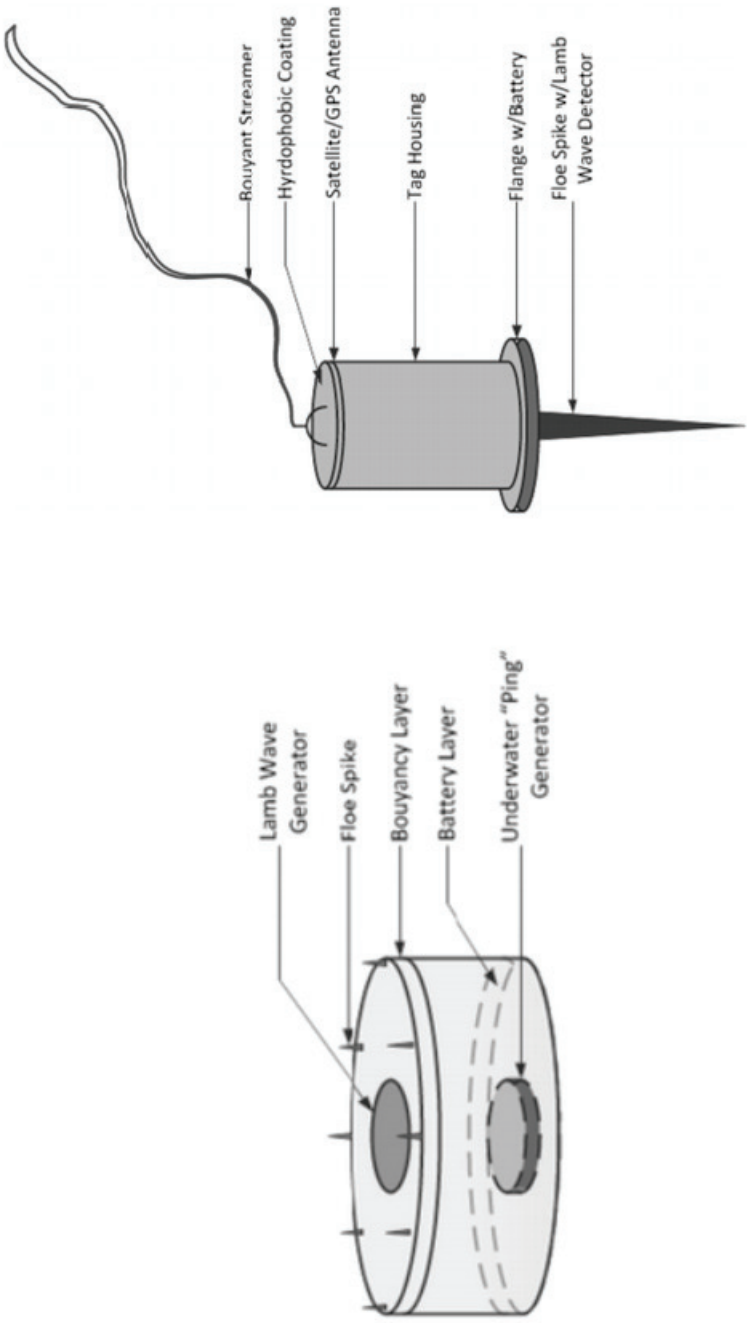

Figure 3: The UWID tag (left) generates an acoustic signal below the ice, which is picked up by the LD-GRIDSAT (right) on the surface of the ice, Source: URS Group [3]

In 2013, Stan Dosso determined the location of an underwater acoustic source using hydrophones on the surface of the ice [4-6]. In Dosso's experiment the acoustic source was submerged deep in the water, and the sound waves primarily traveled through water. In our case the acoustic source will touch the bottom of the iceberg, and the sound waves will primarily travel through the ice. Also, while Dosso determined the depth of the acoustic source by looking at the attenuation of the signal, our method will focus on the time of arrival to the hydrophone.

2 Lamb Wave Behavior

In our system, the acoustic source under the ice will create Lamb waves, sound waves that propagate through solid plates. Horace Lamb first described the properties of Lamb waves in 1917 [7]. Lamb waves are comprised of a combination of asymmetric (flexural) and symmetric (extensional) modes. These modes are typically plotted on dispersion curves, which relate the phase velocity or group velocity of the modes to the frequency of the wave multiplied by the thickness of the plate. The behavior of Lamb waves through a given medium can be analytically determined using the longitudinal velocity and the shear velocity of sound in a given medium.

We choose a coordinate system shown in Figure 4, with the Lamb waves propagating in the x direction, with the condition that the element of the stresses σ_{zz}, σ_{zy}, σ_{zx} are all equal to zero when $z = \pm d$.

The solution to the displacement vector can be separated into two components, according to the Helmholtz decomposition:

$$\vec{u} = \nabla\phi + \nabla \times \psi \tag{2.1}$$

where ϕ is the longitudinal component and ψ is the shear component of the displacement vector. For plane strain, the equations to the longitudinal and shear components

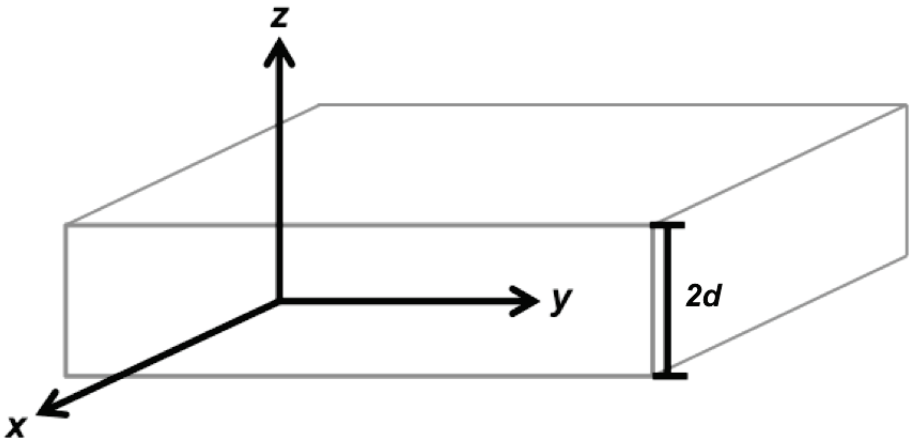

Figure 4: The coordinate system used for our model, where $2d$ is the thickness of the ice. In this system, the wave propagates in the x direction.

of the particle displacements are as follows:

$$\frac{1}{c_L}\frac{\partial^2\phi}{\partial t^2} = \nabla^2\phi = \frac{\partial^2\phi}{\partial x^2} + \frac{\partial^2\phi}{\partial z^2} \tag{2.2}$$

$$\frac{1}{c_T}\frac{\partial^2\psi}{\partial t^2} = \nabla^2\psi = \frac{\partial^2\psi}{\partial x^2} + \frac{\partial^2\psi}{\partial z^2} \tag{2.3}$$

where c_L and c_T are the velocities of longitudinal and shear waves in the material, respectively. In longitudinal waves, particles in the material move parallel to the direction of propagation. In shear waves, the particles move perpendicular to the direction of propagation.

The solutions to the longitudinal and shear components of the material are as follows, using the constants defined by Joseph Rose in *Ultrasonic Waves in Solid Media* [8]:

$$\phi = (A_1\sin(pz) + A_2\cos(pz))e^{i(kx-\omega t)} \tag{2.4}$$

$$\psi = (B_1\sin(qz) + B_2\cos(qz))e^{i(kx-\omega t)} \tag{2.5}$$

where

$$p^2 = \frac{\omega^2}{c_L^2} - k^2 \tag{2.6}$$

$$q^2 = \frac{\omega^2}{c_T^2} - k^2 \tag{2.7}$$

$$k = \frac{2\pi}{\lambda} = \frac{\omega}{c_P} \tag{2.8}$$

Here ω is the circular frequency and c_P is the phase velocity of the Lamb wave mode.

The particle velocities and the stress tensors can be found in terms of the displacement vectors, using the strain equations (2.4) and (2.5).

$$u = \frac{\partial \phi}{\partial x} + \frac{\partial \psi}{\partial z} \tag{2.9}$$

$$v = 0 \tag{2.10}$$

$$w = \frac{\partial \phi}{\partial z} - \frac{\partial \psi}{\partial x} \tag{2.11}$$

$$\sigma_{zx} = \mu \left(\frac{\partial^2 \phi}{\partial x \partial z} - \frac{\partial^2 \psi}{\partial x^2} + \frac{\partial^2 \psi}{\partial z^2} \right) \tag{2.12}$$

$$\sigma_{zz} = \lambda \left(\frac{\partial^2 \phi}{\partial x^2} + \frac{\partial^2 \phi}{\partial z^2} \right) + 2\mu \left(\frac{\partial^2 \phi}{\partial z^2} + \frac{\partial^2 \psi}{\partial x \partial z} \right) \tag{2.13}$$

where μ and λ are Lamé constants. u, v, and w are the particle velocities in the x, y, and z directions, respectively.

These differential equations yield the following asymetric and symmetric solutions:

Symmetric Modes:

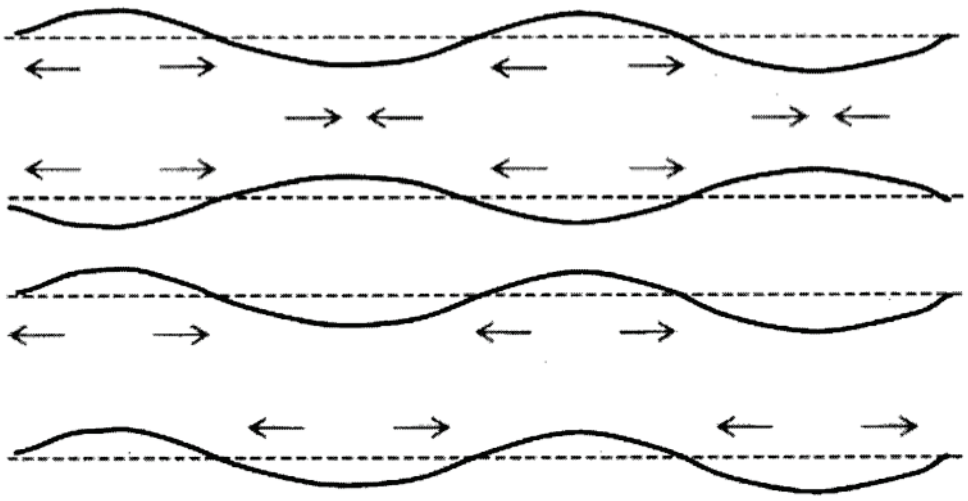

Figure 5: The solutions to the Lamb wave boundary conditions yield symmetric modes (top) and asymmetric modes (bottom), Source: Khine and Tsai [9]

$$u = ikA_2 \cos(pz) + bqB_1 \cos(qz)$$

$$w = -pA_2 \sin(pz) - ikB_1 \sin(qz)$$

$$\sigma_{zx} = \mu(-2ikpA_2 \sin(pz) + (k^2 - q^2)B_1 \sin(qz))$$

$$\sigma_{zz} = -\lambda(k^2 + p^2)A_2 \cos(pz) - 2\mu(p^2 A_2 \cos(pz) + ikqB_1 \cos(qz))$$

Asymmetric Modes:

$$u = ikA_1 \sin(pz) - qB_2 \sin(qz)$$

$$w = pA_1 \cos(pz) - ikB_2 \cos(qz)$$

$$\sigma_{zx} = \mu(2ikpA_1 \cos(pz) + (k^2 - q^2)B_2 \cos(qz))$$

$$\sigma_{zz} = -\lambda(k^2 + p^2)A_1 \sin(pz) - 2\mu(p^2 A_1 \sin(pz) + ikqB_2 \sin(qz))$$

Diagrams of asymmetric and symmetric waves are shown in Figure 5.

Applying these solutions to the boundary condition allow us to determine the final equations for the Lamb waves:

Symmetric Modes:

$$\frac{\tan(qh)}{\tan(ph)} = -\frac{4k^2pq}{(q^2-k^2)^2} \tag{2.14}$$

Asymmetric Modes:

$$\frac{\tan(qh)}{\tan(ph)} = -\frac{(q^2-k^2)^2}{4k^2pq} \tag{2.15}$$

The equations can be used to generate dispersion curves, which give phase velocity (the velocity of individual particles) and group velocity (the velocity of a wave packet) as a function of frequency-thickness product in Lamb waves. Example dispersion curves for an aluminium plate are shown in Figure 6.

As Figure 6 shows, dispersion curves are divided into symmetric modes (S0, S1, S2...) and asymmetric modes (A0, A1, A2...). Note that the zeroth order dispersion curve for phase velocity flattens and approaches a constant value as the frequency-distance product approaches zero. Computers can generate the dispersion curves for a material given its density, longitudinal velocity, and shear velocity.

Previous research has examined the longitudinal and shear velocites of sound in ice. In 1934, Ewing, Crary, and Thorne measured the longitudinal velocity, shear velocity, and Young's modulus of pure ice [10]. In 1950, Press and Ewing modeled the dispersion curve of ice sheets floating in water, with an acoustic source above or below the ice [11]. While these models can provide a general guide for our research, the acoustic properties of sea ice will be different from pure ice. In 2014, Gao et al. used these models to detect flaws in solid plates floating above water [12].

The longitudinal and shear velocity of sound waves in sea ice vary with temperature. Over the course of five months, Kenneth Hunkins studied elastic wave propagation in arctic ice, measuring the longitudinal and shear velocities of sound in ice during the months of August, September, January, March, and April [13]. Hunk-

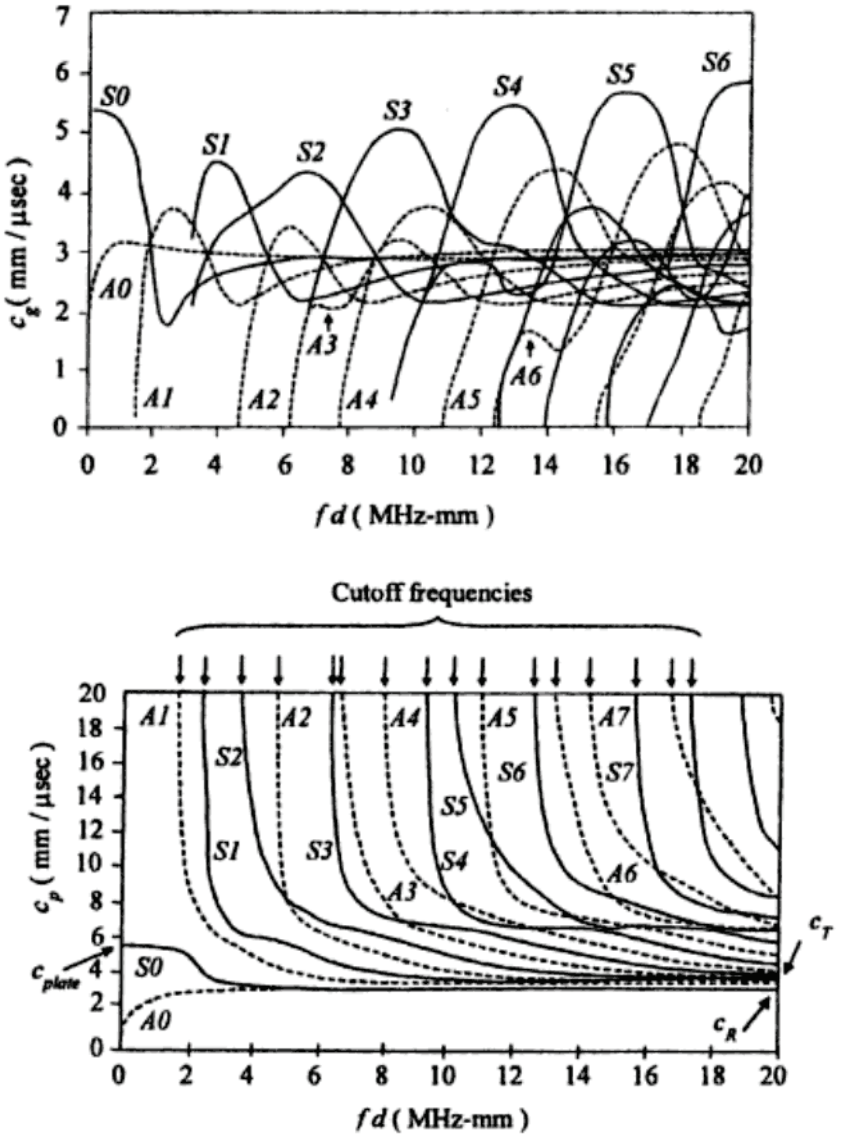

Figure 6: Dispersion curves of an aluminum plate for group velocity (top) and phase velocity (bottom), Source: Khine and Tsai [7]

ins found that longitudinal plate wave velocity varied from 2457 m/s in August to 3181 m/s in January. Shear velocity varied from 1552 m/s in August to 1862 m/s in January.

In addition, shear wave velocity in ice can vary with depth. Wittlinger and Farra found that the vertical shear velocity in Antarctic and Greenland ice sheets dramatically decreases at the bottom of the ice [14]. They measured an average shear velocity of 2030 m/s in the upper ice layer and a shear velocity of 1560 m/s in the lower ice layer.

In 1972, Kohnen experimentally determined the plate wave velocity, shear wave velocity, and density of sea ice in Baffin Island, Canada [15]. He used these measurements to calculate the Young's modulus, shear modulus, and Poisson's ratio of arctic sea ice. In 1982 Blanchet, Abdelnour, and Comfort calculated flexural strength data of sea ice in the Beaufort Sea, Canada [16]. They were able to model the elastic modulus of first year sea ice as a function of salinity and temperature.

In 1994, Xie and Farmer experimentally measured the shear and longitudinal velocities of sound in first year sea ice [17]. They found that shear wave velocity is more consistent than longitudinal waves—shear wave velocity had a variability of 13%, while longitudinal wave velocity had a variability of 27%. However, Xie and Farmer found that variability increases significantly when the sound waves travel through sea ice pressure ridges, caused by the collision of ice floes.

3 Dispersion Curves for Sea Ice

In 2009, Claudio Strobbia et al. used a point-receiver system to analyze the seismic properties of arctic Russian geography [18]. A part of their research involved studying of properties of sound traveling through lakes where the surface is frozen. Anurupa Shaw and Nico Declereq used Lamb waves to measure the thickness of ice suspended

over a lake [19]. In both cases, the researchers generated dispersion curves of arctic ice in order to predict the behavior of sound through a plate of ice.

In order for our system to function with real-world iceberg, it must be able to detect and analyze Lamb waves where the shear and longitudinal velocities of the ice fall within a realistic range. We used a program designed by Jose Luis Prego, The LAMB Toolbox, to map out the possible dispersion curves for Lamb waves in arctic ice [20]. By manipulating the range of possible longitudinal and shear velocities, we were able to look at the most extreme cases—where the possible longitudinal and shear velocities are either at their maximum or minimum. We used the data from Hunkins's experiment to model the dispersion curves of Lamb waves in ice under in four extreme situations: maximum longitudinal velocity with maximum shear velocity, maximum longitudinal velocity with mimimum shear velocity, minimum longitudinal velocity with maximum shear velocity, and minimum longitudinal velocity and minimum shear velocity [13].

Also shown on the dispersion curves are the Rayleigh wave velocities. Rayleigh waves travel at the surface of the ice, while Lamb waves travel through the center of the ice. As the dispersion curves in this section show, the the zeoth order symmetric and asymmetric modes converge toward the Rayleigh wave velocity as the frequency-thickness product value increases.

3.1 Phase Velocity Dispersion Curves

In phase velocity dispersion curves, the zeroth order symmetric mode flattens when the frequency-thickness product value is close to 0 Hz*m, while the zeroth order asymmetric mode curves downward and approaches 0 m/s as the frequency-thickness product value is close to 0 Hz*m. In our experiment, it will be convenient to work with a region where the dispersion curve slope is close to zero, because the waves will approach the accelerometer at a fixed velocity, regardless of small shifts in fre-

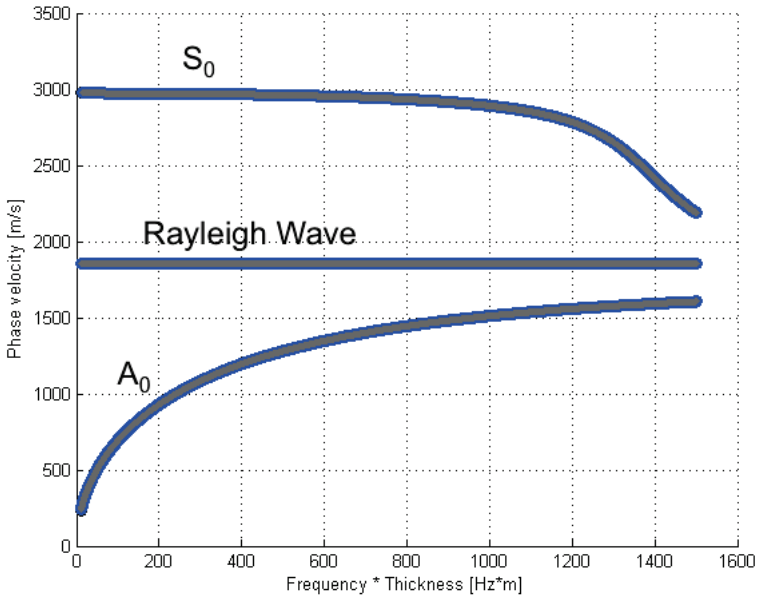

Figure 7: Phase velocity dispersion curve for ice with maximum longitudinal velocity and maximum shear velocity

quency or ice thickness. For this reason, we will use the zeroth order symmetric mode as a reference point, because it flattens and approaches a fixed constant when the frequency-thickness product value approaches zero. Choosing a region where the frequency is low is beneficial for three other reasons. First, low frequency acoustic waves travel further, increasing the range of our triangulation system. Second, low frequency waves are less sensitive to irregularities in the ice, so the waves will travel with more consistency. Third, the higher order symmetric modes will be cut off at lower frequencies, allowing us to focus on the lower order symmetric modes.

The phase velocity dispersion curves (Figures 7 through 10) show the relationship between frequency, thickness, and phase velocity of Lamb waves in ice floes. We will use the phase velocity to determine the appropriate angle of incidence to generate the Lamb waves.

As Figures 7-10 show, the range of possible longitudinal and shear velocities allows

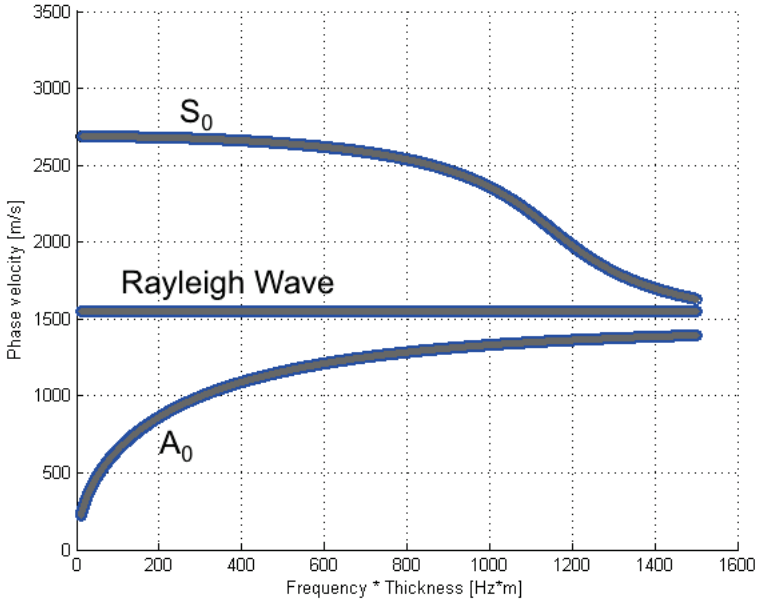

Figure 8: Phase velocity dispersion curve for ice with maximum longitudinal velocity and minimum shear velocity

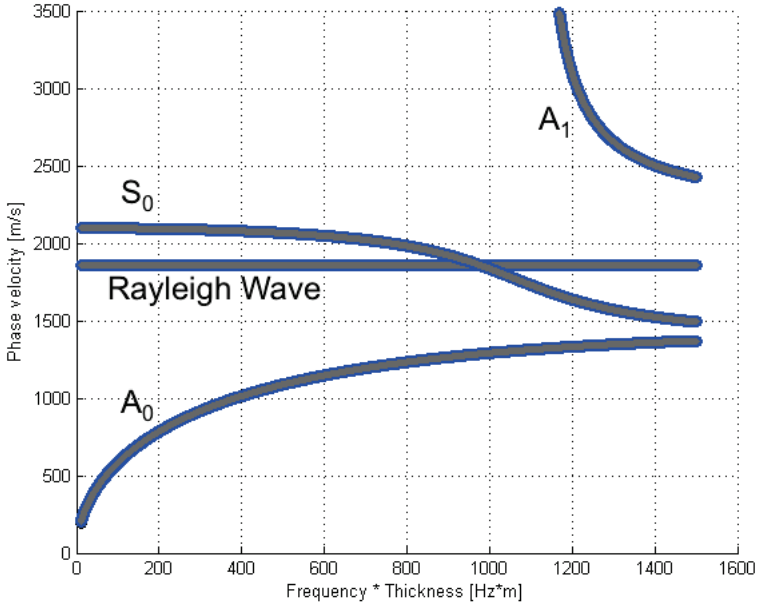

Figure 9: Phase velocity dispersion curve for ice with minimum longitudinal velocity, maximum shear velocity

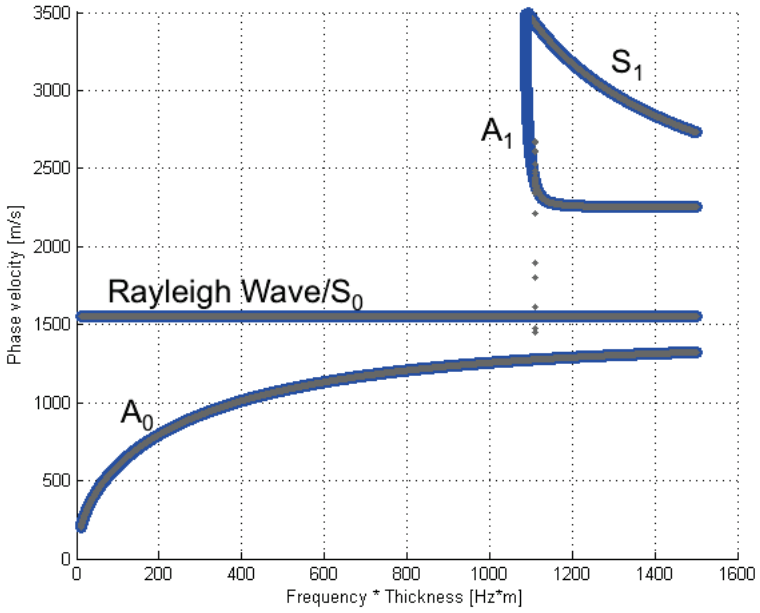

Figure 10: Phase velocity dispersion curve for ice with minimum longitudinal velocity, minimum shear velocity

for significant variation between the dispersion curves. In the case where we consider the minimum longitudinal and shear velocities (Figure 10), the zeroth order mode is low enough that it is indistinguishable from the Rayleigh wave velocity.

Previous studies of Lamb waves (e.g. Gao et al. [12], Imano and Endo [21]) have used Snell's law to determine the ideal incident angle of the incoming sound wave to most effectively create Lamb waves in a plate:

$$\sin\theta = \frac{c_w}{c_p} \tag{3.1}$$

where c_w is the speed of sound in the material that the incoming sound wave propagates through, and c_p is the phase velocity in the solid plate. In our case, c_w is the speed of sound in arctic seawater, while c_p is the phase velocity of sound in ice for the zeroth order symmetric mode as frequency-thickness product approaces zero, as determined by our dispersion curves. The possible phase velocities as frequency

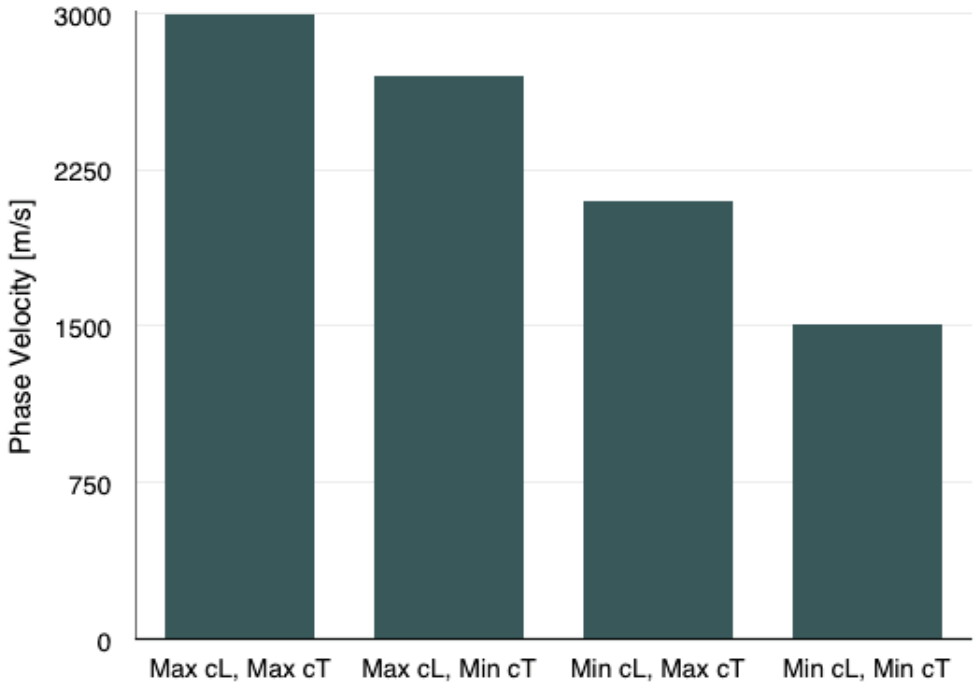

Figure 11: Phase velocity of the zeroth order symmetric mode when frequency-thickness product is close to zero in four different cases: (1) maximum longitudinal velocity with maximum shear velocity, (2) maximum longitudinal velocity with minimum shear velocity, (3) minimim longitudinal velocity with maximum shear velocity, and (4) minimum longitudinal velocity with minimum shear velocity

approaches zero is shown in Figure 11, with data drawn from Figures 7-10. The speed of sound in arctic water was calculated using the equations decribed by Dushaw et al. in *On equations for the speed of sound in seawater* [22]. Variation in the phase velocity does not significantly change the value of the incident angle, which will be approximately 24°, according to equation (3.1).

3.2 Group Velocity Dispersion Curves

The group velocity dispersion curves (Figures 12 through 15) show the relationship between frequency, thickness, and group velocity of Lamb wave in ice floes. The group velocity dispersion curves will allow us to determine the time it takes the signal to travel from the acoustic source under the ice (the UWID tag) to the receivers

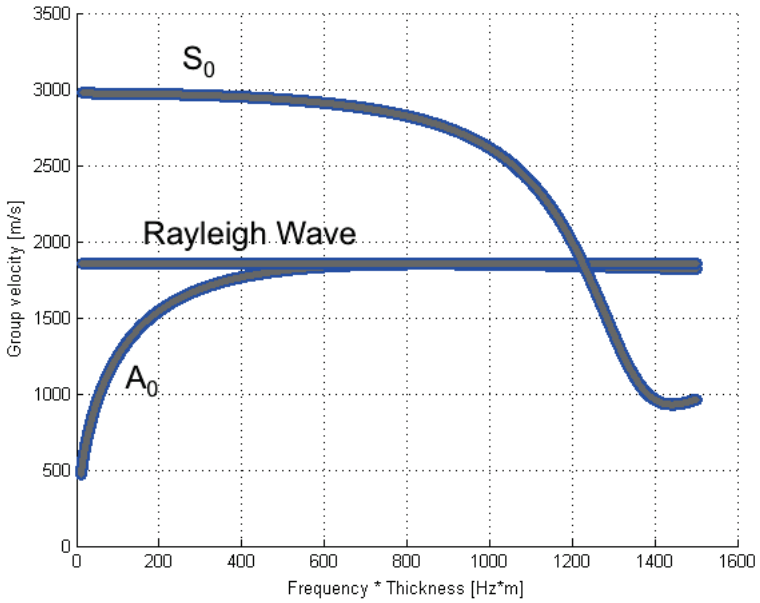

Figure 12: Group velocity dispersion curve for ice with maximum longitudinal velocity, maximum shear velocity

embedded in the surface of the ice (the LD-GRIDSAT). This information will be necessary for triangulating the location of the underwater acoustic source, allowing the cleanup crew to approximate the location of the oil slick.

As Figures 12-15 show, the range of possible longitudinal and shear velocities for ice leads to a range of group velocities between 3000 m/s and 1500 m/s, which is similar to the range of phase velocities. As with the phase velocity dispersion curves, the zeroth order mode is low enough that it is indistinguishable from the Rayleigh wave velocity.

In future research, we will use the group velocity information to develop a system that can automatically triangulate the location of the acoustic source, using the GPS coordinates of the acoustic receivers and the difference in receiving time for the different acoustic receivers. Previous studies have developed techniques for triangulating the location of acoustic sources in plate-like structures [23-28]. The general equation

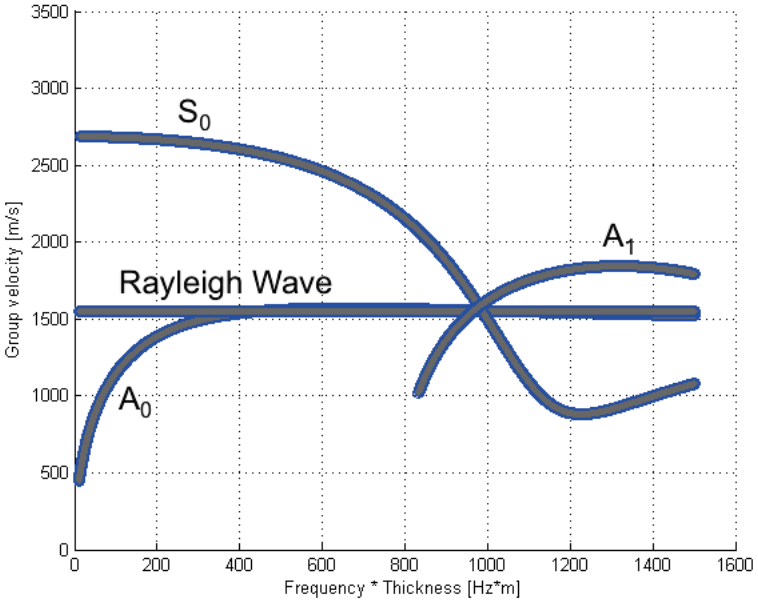

Figure 13: Group velocity dispersion curve for ice with maximum longitudinal velocity, minimum shear velocity

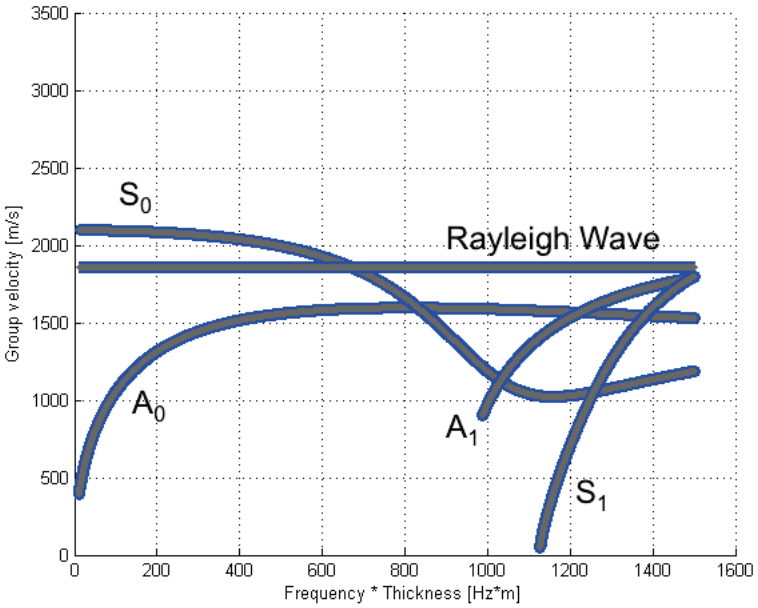

Figure 14: Group velocity dispersion curve for ice with minimum longitudinal velocity, maximum shear velocity

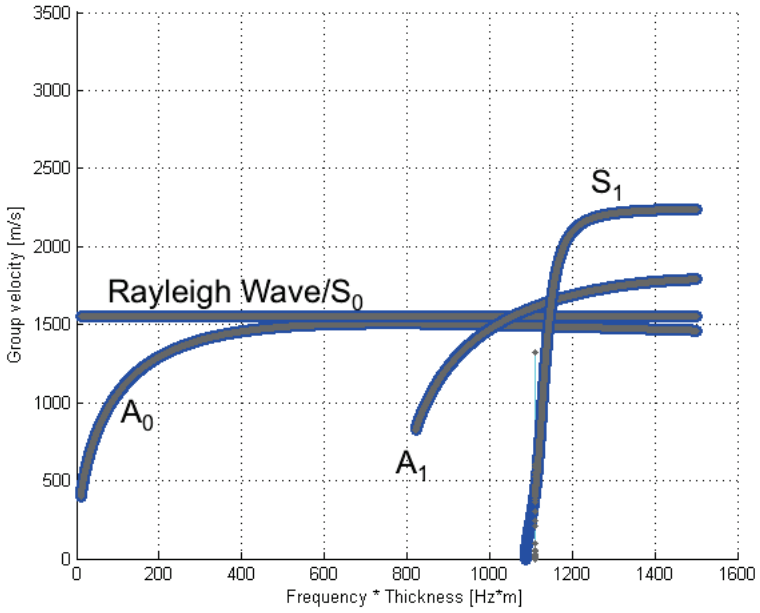

Figure 15: Group velocity dispersion curve for ice with minimum longitudinal velocity, minimum shear velocity

relating the location of the source to the time difference between different acoustic receivers detecting the signal is below:

$$\Delta t_{ij} = \frac{\sqrt{(x_d - x_i)^2 - (y_d - y_i)^2} - \sqrt{(x_d - x_j)^2 - (y_d - y_j)^2}}{v_g} \tag{3.2}$$

where (x_d, y_d) is the coordinates for the acoustic source, (x_i, y_i) and (x_j, y_j) are the coordinates for the receivers, Δt_{ij} is the time difference between the ith and jth receiver detecting the signal, and v_g is the phase velocity, as shown in Figure 16.

4 Finite Difference Time Domain Analysis

Now that we have determined the proper angle of incidence to strike the ice, further analysis is needed to predict the behavior of the sound wave propagating through the sea ice. In the next part of our research, we used Finite Difference Time Domain

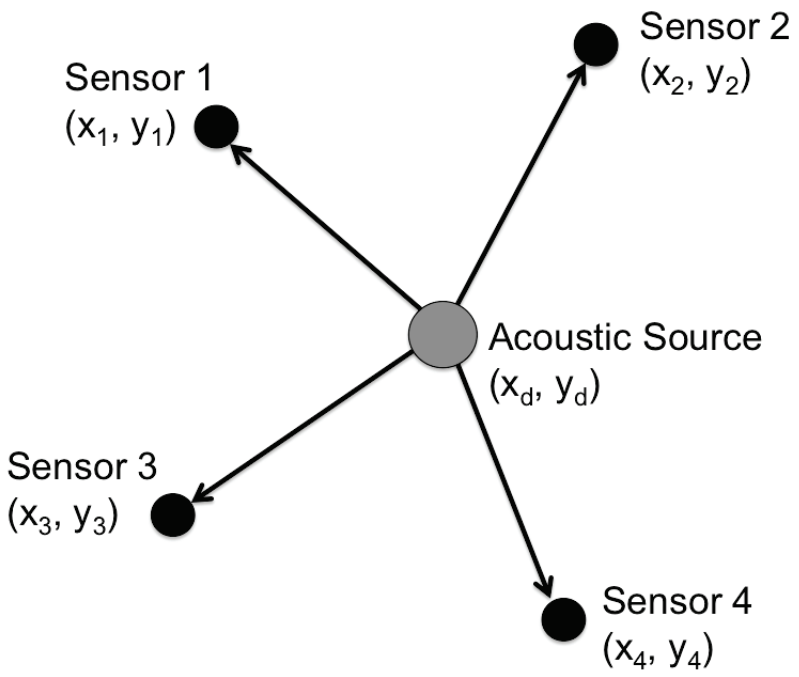

Figure 16: Using several receivers scattered on the ice, the location of an acoustic source can be triangulated

Analysis to model the behavior of the sound wave through a slab of ice floating on water.

The finite difference time domain method uses numerical analysis to solve wave equations by replacing derivatives with finite differences, for example:

$$\frac{\partial f}{\partial x} = \frac{f(x_0 + \frac{\delta}{2}) - f(x_0 - \frac{\delta}{2})}{\delta} \tag{4.1}$$

In 1966, Kane Yee used finite difference equations as a substitute for Maxwell's equations to describe the behavior of electromagnetic pulses [29]. Since then, Yee's FDTD methods have been modified to describe acoustic propagation [30-33]. Narayan and Sahar used FDTD code to model the behavior of viscoelastic geological materials [34].

We begin with basic wave equations for acoustics:

$$\frac{\partial P}{\partial t} = -\rho c^2 \nabla \cdot \mathbf{v} \tag{4.2}$$

$$\frac{\partial \mathbf{v}}{\partial t} = -\frac{1}{\rho} \nabla P \tag{4.3}$$

where P is the pressure, c is the speed of sound, $\mathbf{v}$ is the velocity of an individual particle, and ρ is the density of the material.

We can expand these equations in terms of the components:

$$\frac{\partial P}{\partial t} = -\rho c^2 \left(\frac{\partial v_x}{\partial x} + \frac{\partial v_y}{\partial y} + \frac{\partial v_z}{\partial z} \right) \tag{4.4}$$

$$\frac{\partial v_x}{\partial t} = -\frac{1}{\rho} \frac{\partial P}{\partial x} \tag{4.5}$$

$$\frac{\partial v_y}{\partial t} = -\frac{1}{\rho} \frac{\partial P}{\partial y} \tag{4.6}$$

$$\frac{\partial v_z}{\partial t} = -\frac{1}{\rho}\frac{\partial P}{\partial z} \tag{4.7}$$

In the acoustic TDFD model described by John Schneider in *Understanding the Finite-Difference Time-Domain Method*, the pressure node is assumed to be half a temporal step from the velocity nodes, and the three velocity components are half a spatial step from the pressure node [35]. Using finite differences, the pressure and velocity components become:

$$P(x, y, z, t) = P(m\delta_x, n\delta_y, p\delta_z, q\delta_t) = P^q[m, n, p] \tag{4.8}$$

$$v_x(x, y, z, t) = v_x([m + 1/2]\delta_x, n\delta_y, p\delta_z, [q + 1/2]\delta_t) = v_x^{q+1/2}[m, n, p] \tag{4.9}$$

$$v_y(x, y, z, t) = v_x(m\delta_x, [n + 1/2]\delta_y, p\delta_z, [q + 1/2]\delta_t) = v_y^{q+1/2}[m, n, p] \tag{4.10}$$

$$v_x(x, y, z, t) = v_x(m\delta_x, n\delta_y, [p + 1/2]\delta_z, [q + 1/2]\delta_t) = v_z^{q+1/2}[m, n, p] \tag{4.11}$$

where (m, n, p, q) is the initial value of (x, y, z, t), as shown in Figure 10. We also assume the spatial step sizes are the same, so $\delta_x = \delta_y = \delta_z = \delta$.

Combining the finite difference approximations with equation (4.4), we have an updated equation for pressure:

$$P[m, n, p] = P^{q-1}[m, n, p] - \rho c^2 \frac{\delta_t}{\delta}(v_z^{q-1/2}[m, n, p] - v_z^{q-1/2}[m - 1, n, p] + v_y^{q-1/2}[m, n, p] - v_y^{q-1/2}[m, n - 1, p] + v_z^{q-1/2}[m, n, p] - v_z^{q-1/2}[m, n, p - 1] \tag{4.12}$$

We can then use the updated pressure equation to find finite difference solutions

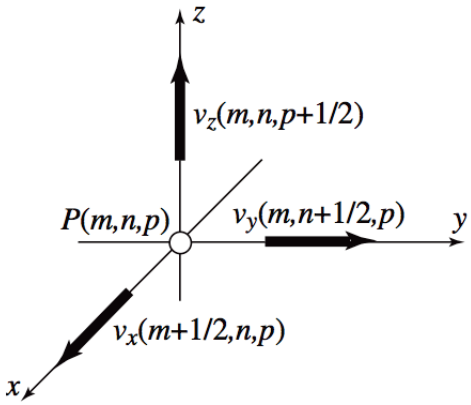

Figure 17: Acoustic particle in three dimensions, according to the finite difference time domain model, John Schneider [35].

for the velocity components:

$$v_x^{q+1/2}[m,n,p] = v_x^{q-1/2}[m,n,p] - \frac{2\delta_t}{\delta}\frac{(P^q[m+1,n,p] - P^q[m,n,p])}{\rho[m,n,p] + \rho[m+1,n,p]} \tag{4.13}$$

$$v_y^{q+1/2}[m,n,p] = v_y^{q-1/2}[m,n,p] - \frac{2\delta_t}{\delta}\frac{(P^q[m,n+1,p] - P^q[m,n,p])}{\rho[m,n,p] + \rho[m,n+1,p]} \tag{4.14}$$

$$v_z^{q+1/2}[m,n,p] = v_z^{q-1/2}[m,n,p] - \frac{2\delta_t}{\delta}\frac{(P^q[m,n,p+1] - P^q[m,n,p+1])}{\rho[m,n,p+1] + \rho[m,n,p+1]} \tag{4.15}$$

Bolmer and Stephen used these methods to develop the GeoAcoustic_TDFD software package, which models the propagation of sound waves through layered media. GeoAcoustic_TDFD was originally designed to model acoustic sources above the sea floor, but we modified the code so it modeled an acoustic source under an ice floe. We specified the density, phase velocity, and group velocity of the layers: water at the bottom, ice in the middle, and air at the top.

Figures 18-24 model the sound wave propagating through the layered system at intervals of 0.1 seconds.

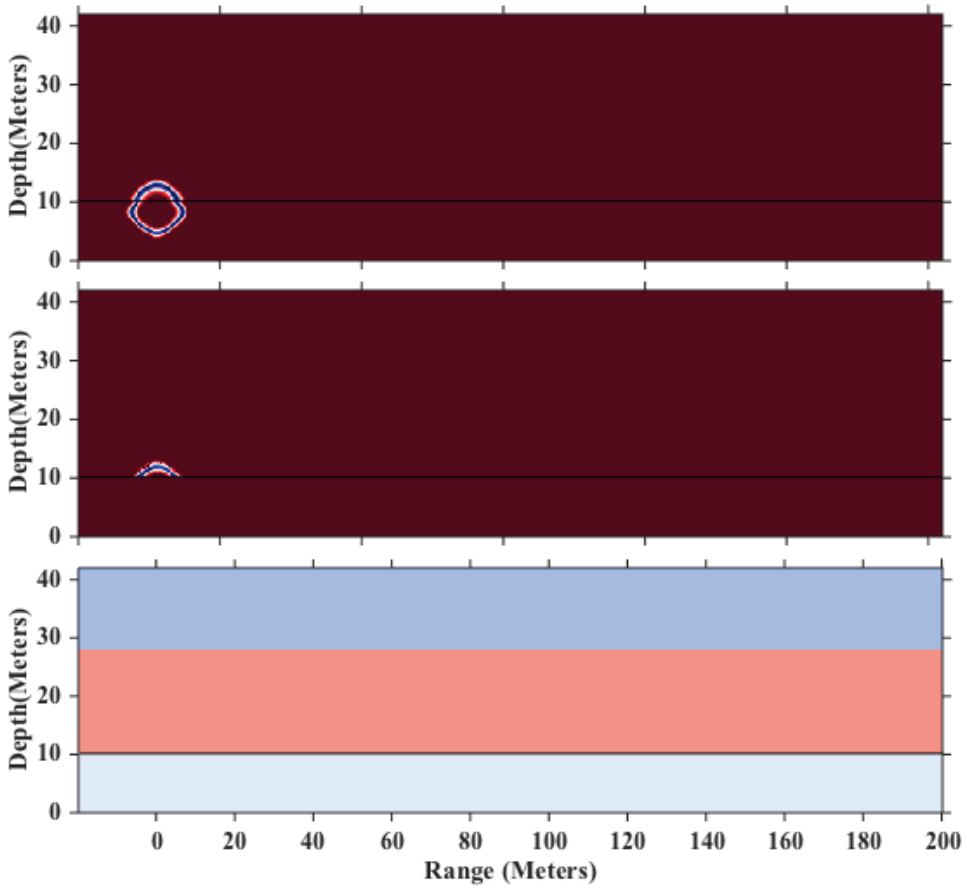

Figure 18: FDTD model of sound wave in layered system after .01 seconds. The top graph shows the intensity of longitudinal waves, the middle graph shows the intensity of shear waves, and the bottom graph marks the distinction between the air, the ice, and the ocean water. High intensity regions are shown in blue, while low intensity regions are shown in dark red.

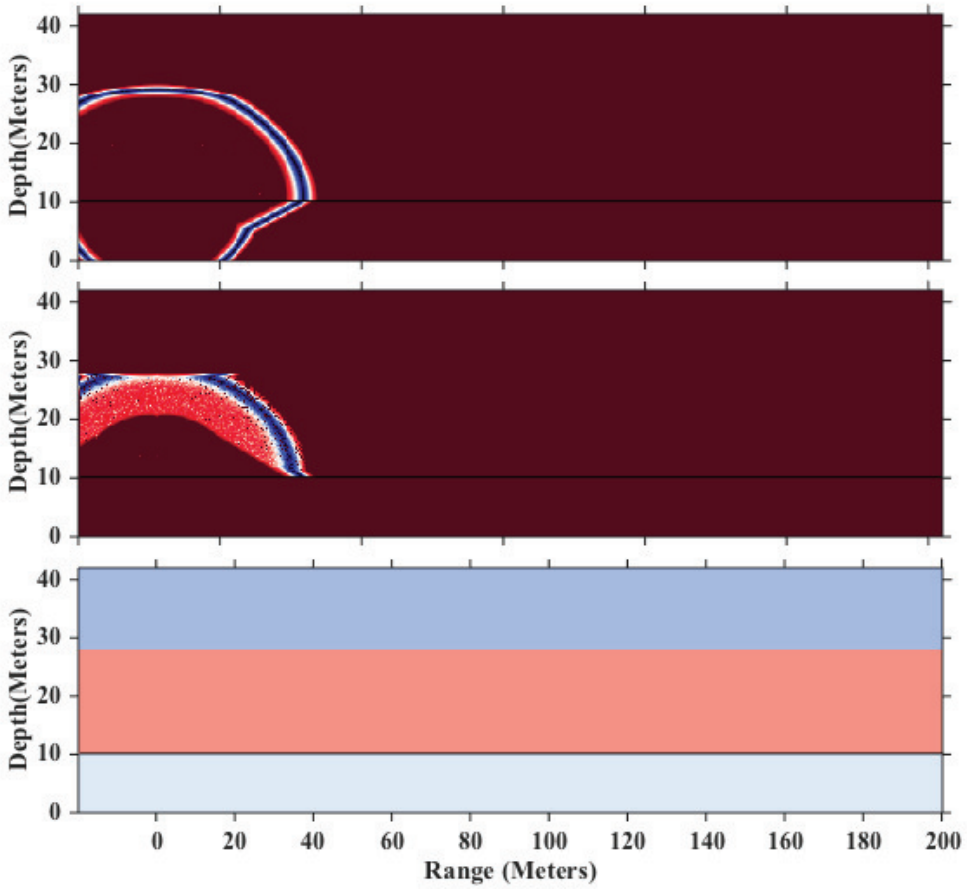

Figure 19: FDTD model of sound wave in layered system after .06 seconds. The top graph shows the intensity of longitudinal waves, the middle graph shows the intensity of shear waves, and the bottom graph marks the distinction between the air, the ice, and the ocean water. High intensity regions are shown in blue, while low intensity regions are shown in dark red.

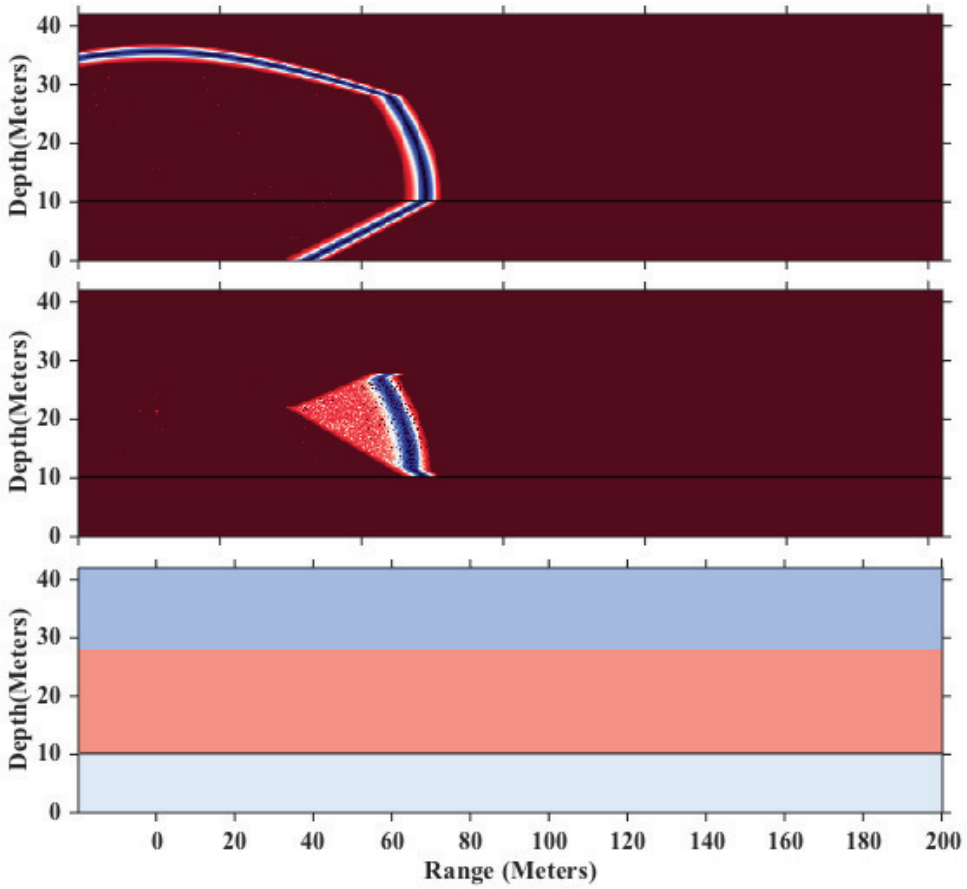

Figure 20: FDTD model of sound wave in layered system after .11 seconds. The top graph shows the intensity of longitudinal waves, the middle graph shows the intensity of shear waves, and the bottom graph marks the distinction between the air, the ice, and the ocean water. High intensity regions are shown in blue, while low intensity regions are shown in dark red.

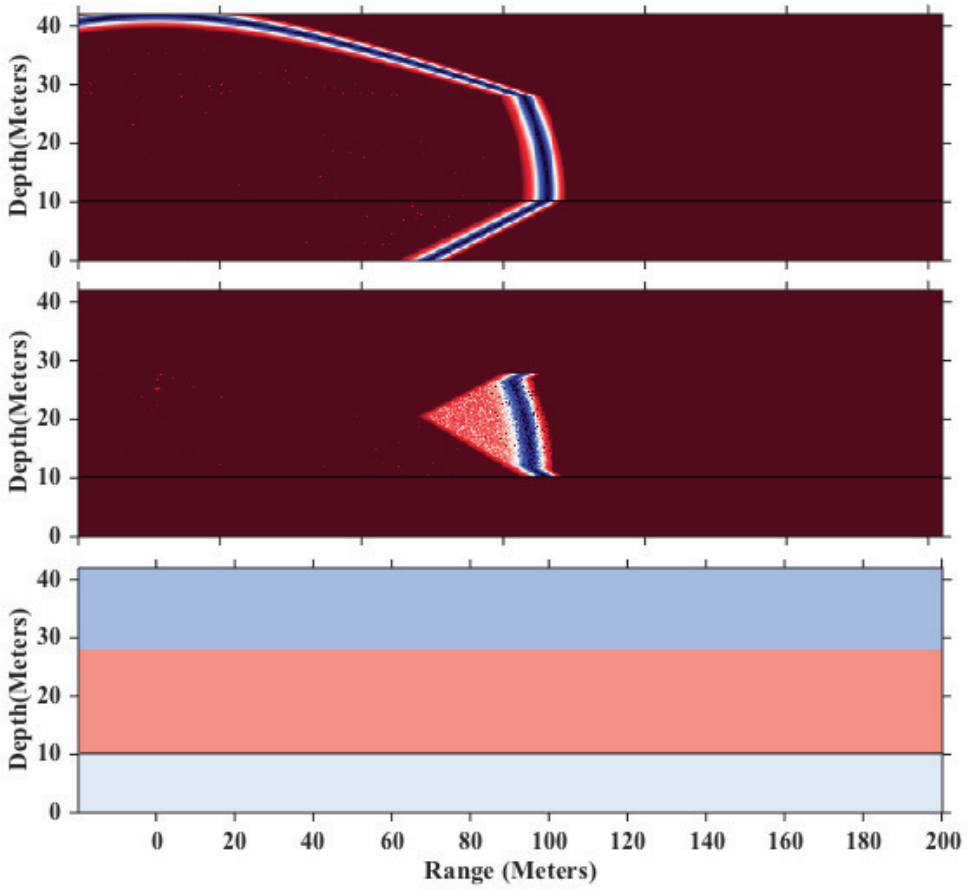

Figure 21: FDTD model of sound wave in layered system after .16 seconds. The top graph shows the intensity of longitudinal waves, the middle graph shows the intensity of shear waves, and the bottom graph marks the distinction between the air, the ice, and the ocean water. High intensity regions are shown in blue, while low intensity regions are shown in dark red.

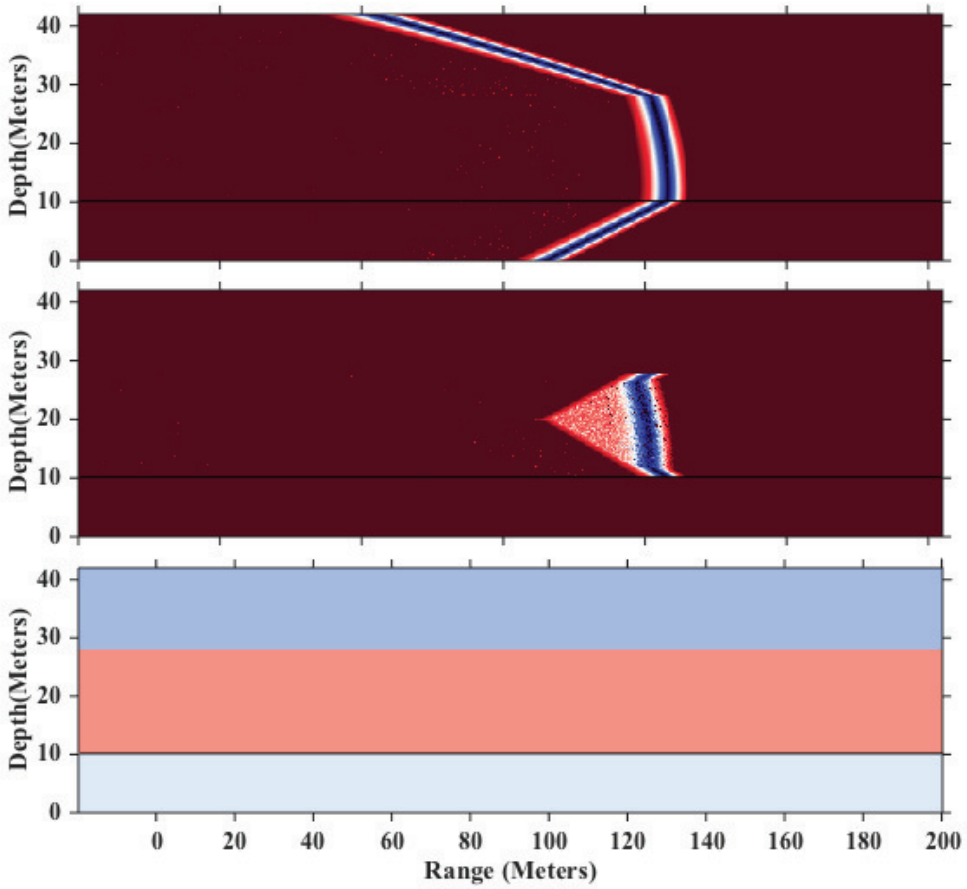

Figure 22: FDTD model of sound wave in layered system after .21 seconds. The top graph shows the intensity of longitudinal waves, the middle graph shows the intensity of shear waves, and the bottom graph marks the distinction between the air, the ice, and the ocean water. High intensity regions are shown in blue, while low intensity regions are shown in dark red.

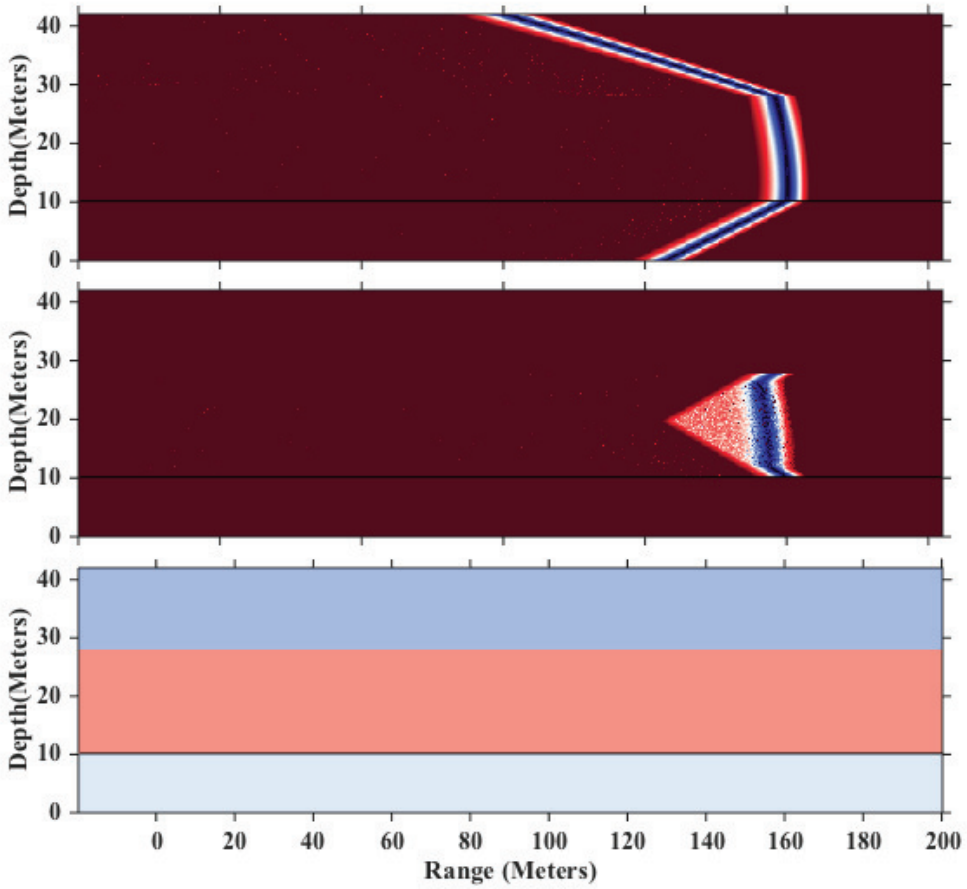

Figure 23: FDTD model of sound wave in layered system after .26 seconds. The top graph shows the intensity of longitudinal waves, the middle graph shows the intensity of shear waves, and the bottom graph marks the distinction between the air, the ice, and the ocean water. High intensity regions are shown in blue, while low intensity regions are shown in dark red.

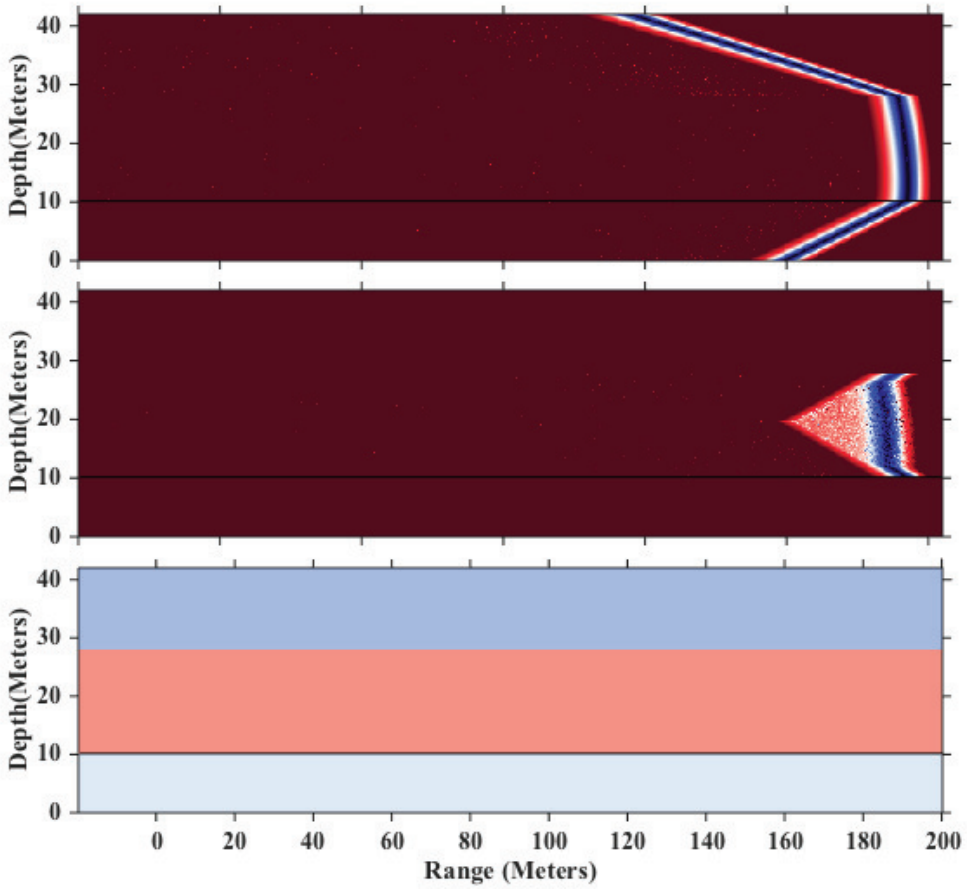

Figure 24: FDTD model of sound wave in layered system after .31 seconds. The top graph shows the intensity of longitudinal waves, the middle graph shows the intensity of shear waves, and the bottom graph marks the distinction between the air, the ice, and the ocean water. High intensity regions are shown in blue, while low intensity regions are shown in dark red.

As Figures 18 demonstrates, the initial acoustic signal only has longitudinal components, because shear waves do not propagate underwater. Once the initial spherical pulse hits the ice-water boundary, the wave propagates through the ice in the form of both longitudinal waves and shear waves (Figure 19). Once the wave reaches the ice-air boundary, the only longitudinal waves propagate through the air, because air does not carry shear waves (Figure 20).

The longitudinal wave reflects across the water-ice boundary and refracts across the water-air boundary, creating trails following behind the longitudinal wave in the ice, as shown in Figures 20-24. The reflection of the shear wave off the ice-air boundary interacts with the initial shear wave to create the triangle-shaped shear wave impulse shown in Figures 20-24.

5 Conclusion

We studied the behavior of Lamb waves in sea ice in order to develop a system enabling oil cleanup crews to locate the position of an acoustic emitter under the ice, allowing them to locate the underwater oil. By varying the range of possible longitudinal and shear velocities of arctic ice, we were able to generate dispersion curves for group velocity and phase velocity as a function of plate thickness*frequency. We focused our analysis on the zeroth order symmetric mode, which flattens as frequency-thickness product approaches zero, allowing for a system where slight changes in plate thickness will not alter the phase velocity and group velocity.

We also used Finite Difference Time Domain software to model the behavior of the sound waves in the ice, water, and air. As Figures 18-24 show, the interaction between the three layers leads to a vertical longitudinal wave that travels in the ice, trailed by longitudinal waves in the air above and the water below. The reflection of the shear wave off the ice-air boundary interacts with the initial shear wave to create

the triangle-shaped shear wave impulse.

References Cited

1. Joel Achenbach and David A. Fahrenthold, (2010). *Oil spill dumped 4.9 million barrels into Gulf of Mexico, latest measure shows*, The Washington Post.

2. Michele Fitzpatrick and Peter A. Tebeau, (2013). *Detection of Oil in Water Column: Sensor Design*, Acquisition Directorate Research & Development Center, Distribution Statement A, Department of Homeland of Security.

3. URS Group, Inc, (2014). *Tagging of Oil Under Ice for Future Recovery*, Solicitation No. E14PS00054.

4. Stan Dosso, (2013). *Three-dimensional Acoustic Localization in the Arctic using an Ice-mounted Geophone.* Paper presented at the OCEANS '13 MTS/IEEE Conference in Bergen, Norway, DOI: 10.1109/OCEANS-Bergen.2013.6607963.

5. Stan Dosso, Garry Heard, and Michael Vinnins, (2002). *Source bearing estimation in the Arctic Ocean using ice-mounted geophones*, Journal of the Acoustic Society of America, Vol. 112, #6, pp. 2721-2734.

6. Stan Dosso, Garry Heard, Michael Vinnins, and Slobodan Jovic, (2004). *Field Trials of Geophones as Arctic Acoustic Sensors*, Canadian Acoustics, Vol. 32, #3, pp. 198-199.

7. Horace Lamb, (1917). *On Waves in an Elastic Plate.* Proceedings of the Royal Society of London Series A, Vol. XCIII, pp. 114-128.

8. Joseph Rose, (1999). *Ultrasonic Waves in Solid Media.* Cambridge University Press.

9. Lynn Khine and Ming Lin Julius Tsai, (2013). *Piezoelectric Resonator.* US Patent No. 201008262-6. Washington, DC: U.S. Patent and Trademark Office.

10. Maurice Ewing, A. P. Crary, and A. M. Thorne, (1934). *Propagation of Elastic Waves in Ice. Part I.*, Journal of Applied Physics, Vol. 165, #5, pp. 165-168. 14. P. Crary, (1954). Seismic Studies on Fletcher's Ice Island, T-3, Transactions, American Geophysical Union, Vol. 35, #2, pp. 293-300.

11. Frank Press and Maurice Ewing, (1950). *Theory of Air-Coupled Flexural Waves*, Journal of Applied Physics, Vol. 22, #7, pp. 892-899.

12. G. J. Gao, M. X. Deng, M. L. Li, et al, (2014). *Mode selection of Lamb waves for the evaluation of solid plates with liquid loading*, Science China: Physics, Mechanics & Astronomy, Vol. 57, #10, pp. 1840-1847, DOI: 10.1007/s11433-013-5269-0.

13. Kenneth Hunkins, (1960). *Seismic Studies of Sea Ice*, Journal of Geophysical Research, Vol. 65, #10, pp. 3459-3472.

14. Gérard Wittlinger and Véronique Farra, (2012). *Observation of low shear wave velocity at the base of the polar ice sheets: evidence for enhanced anisotropy*, Geophysical Journal International, Vol. 190, pp. 391-405, DOI: 10.1111/j.1365-246X.2012.05474.x.

15. Kohnen, (1972). *Seismic and ultrasonic measurements on the sea ice of Eclipse Sound near Pond Inlet, N.W.T., on northern Baffin Island*, Polarforschung, Vol. 42, #2, pp. 66-74.

16. Denis Blanchet, Razek Abdelnour, and George Comfort, (1997). *Mechanical Properties of First-Year Sea Ice at Tarsuit Island*, Journal of Cold Regions Engineering, Vol. 11, #1, pp. 59-82.

17. Yunbo Xie and David Farmer, (1994). *Seismic-acoustic sensing of sea ice wave mechanical properties*, Journal of Geophysical Research, Vol. 99, #C4, pp. 7771-7786, DOI: 10.1029/93JC03483.

18. Claudio Strobbia, Anna Glushchenko, Andreas Laake, Peter Vermeer, Stuart Papworth, and Ying Ji, (2009). *Arctic near surface challenges: the point receiver solution to coherent noise and statics,* First Break, Vol. 27, pp. 69-76.

19. Anurupa Shaw and Nico Declereq, (2013). *Session 2pPA: Material Characterization,* Proceedings of Meetings on Acoustics, Vol. 19.

20. Jose Luis Prego "The Lamb Matlab toolbox," first release, version, 3 August 2010. [Online]. Available at http://www.mathworks.com/matlabcentral/fileexchange/28367-the-lamb-toolbox.

21. Kazuhiko Imano and Tomoya Endo, (2012). *Experimental Study on the Model Conversion of Lamb Wave Using a Metal Plate Having a Notch Type Defect*, International Journal of the Society of Materials Engineering for Resources, Vol. 19, pp. 20-23.

22. Brian D. Dushaw, Peter F. Worcester, Bruce D. Conruelle, and Bruce M. Howe, (1992). *On equations for the speed of sound in seawater*, Journal of the Acoustical Society of America, Vol. 93, #1, pp. 255-275, DOI: 10.1121/1.405660.

23. F. Ciampa, M. Meo, (2010). *A new algorithm for acoustic emission localization and flexural group determination in anisotropic structures*, Ultrasonics, Vol. 41, #12, pp. 1777-1786.

24. Bernard Castagnede, Wolfgang Sachse, and Kwang Yul Kim, (1989). *Location of pointlike acoustic emission sources in anisotropic plates*, Journal of the Acoustical Society of America, Vol. 86, #3, pp. 1161-1171.

25. Tribikram Kundu, Hayato Nakatani, and Nobuo Takeda, (2012). *Acoustic source localization in anisotropic plates*, Ultrasonics, Vol. 52, #6, pp. 740-746.

26. Amit Shelke, Ahsan Uddin, and Jinkyu Yang, (2014). *Impact Identification in Sandwich Structures Using Solitary Wave-Supporting Granular Crystal Sensors.* AIAA Journal, Vol. 52, #10, pp. 2283-2290.

27. L. Gaul and S. Hurlebaus, (1997). *Identification of the Impact Location on a Plate Using Wavelets.* Mechanical Systems and Signal Processing, Vol. 12, #6, pp. 783-795.

28. Gang Yan and Jianfei Tang, (2014). *A Bayesian Approach for Localization of Acoustic Emission Source in Plate-Like Structures.* Mathematical Problems in Engineering, Volume 2015 (2015), Article ID 247839.

29. Kane S. Yee, (1966). *Numerical Solution of Initial Coundary Value Problems Involving Maxwell's Equations in Isotropic Media*, Antennas and Propagation, Vol. 14, #3, pp. 302-307.

30. E. Ikata and G. Tay, (1998). *Finite-Difference time domain acoustic-wave algorithm*, Il Nuovo Cimento, Vol. 20, #12, pp. 1779-1793.

31. Shuozhong Wang, (1995). *Finite-difference time-domain approach to underwater acoustic scattering problems*, Journal of the Acoustical Society of Oceanography, Vol. 99, #4, pp. 1924-1931.

32. Ahlem Alia, Hakim Djelouah, and Noureddine Bouaoua, (2004). *Finite-Difference Modeling of the Ultrasonic Field radiated by Circular Transducers.* Journal of Computational Acoustics, Vol. 12, #4, pp. 475-499.

33. J. P. Narayan and D. Sahar, (2014). *Three-dimensional viscoelastic finite-difference code and modeling of basement focusing effects on ground motion characteristics.* Computational Geosciences, Vol. 18, pp. 1023-1047.

34. J. P. Narayan and D. Sahar, (2014). *Three-Dimensional Viscoelastic Finite-Difference Code and Modelling of Basement Focusing Effects on Ground Motion Characteristics*, Computational Geosciences, Vol. 18, #6, pp. 1023-1047.

35. John B. Schneider, (2010). *Understanding the Finite-Difference Time-Domain Method,* www.eecs.wsu.edu/~schneidj/ufdtd.